IEEE Access
Multidisciplinary | Rapid Review | Open Access Journal

Received 6 June 2023, accepted 20 June 2023, date of publication 26 June 2023, date of current version 6 July 2023.

Digital Object Identifier 10.1109/ACCESS.2023.3289717

RESEARCH ARTICLE

I-TAINTED: Identification of Turmeric Adulteration Using the CavIty PerturbatioN Technique and Technology OptimizED Machine Learning

TEJINDER KAUR[1], (Member, IEEE), AXEL GAMEZ[2], JOSE-LUIS OLVERA-CERVANTES[3], BENJAMIN CARRION SCHAEFER[2], (Senior Member, IEEE), AND ALONSO CORONA-CHAVEZ[1], (Senior Member, IEEE)

[1]Electronics Department, Universidad Autonoma de la Ciudad de Mexico, Mexico City 09790, Mexico
[2]Department of Electrical and Computer Engineering, The University of Texas at Dallas, Richardson, TX 75080, USA
[3]Instituto Nacional de Astrofisica, Optica y Electronica, Puebla 72000, Mexico

Corresponding author: Alonso Corona-Chavez (alonsocorona@inaoep.mx)

ABSTRACT In this work we propose a method to detect turmeric adulteration using the Cavity Perturbation Technique (CPT) at 2.4GHz. Two different adulterants are examined (egg-yellow color and starch). We show that when a single adulterant is added, the resonant frequency and unloaded quality factor values follow clear trends as a function of added contaminant. Unfortunately, when the turmeric is adulterated with different concentrations of two adulterants (e.g., a 50% color/50% starch) CPT does not lead to good results. To address this, we also present an automated machine learning flow that dramatically enhances the adulteration detection. The proposed flow has the additional uniqueness that it optimizes the predictive model based on the selected target hardware platform doing technology independent as well as technology dependent model optimizations. Experimental results show that our predictive model can be optimized based on the accuracy required for different hardware platforms. In particular we target a microcontroller and a dedicated hardware implementation.

INDEX TERMS Predictive model, sensor design, tumeric contamination.

I. INTRODUCTION

Turmeric (Curcuma Longa) powder is a well-known spice used worldwide due to its condiment uses, as well as its medicinal properties. Turmeric's main proactive component is a polyphenol, namely, curcumin ($C_{21}\,H_{20}\,O_6$) [1]. In the literature, we find curcuma to have been utilized as an antiviral, antibacterial, antifungal and anti-inflammatory [2], [3]. This latest property has led to treatments for cancer, Alzheimer's disease and rheumatoid arthritis [4], [5].

Adulteration of turmeric has been well documented in the literature. It has been shown that fraudsters often use: ground grass, sawdust, straw, cereals, starches, red brick dust and other Turmeric species (C. zedoaria and C malabarica) [6], [7], [8], [9], [10]. This practice, apart from reducing the food quality and nutritional value, poses a risk to public health.

Different methods to detect adulteration have been proposed in the literature such as chromatography [11], [12], DNA analysis [13] and Near Infrared Spectrometry [14]. In [15] a near infrared spectrometer is used to identify Turmeric's three most common adulterants (corn starch powder, Metanil yellow powder, and Sudan dye- IV). An alternative method that allows adulteration identification is measuring the dielectric properties (DP) at microwave frequencies [16]. Microwave characterization of turmeric has been reported in [17] at various moisture levels using

The associate editor coordinating the review of this manuscript and approving it for publication was Yiqi Liu.

a coaxial probe from 0.2 to 20GHz. In addition, in [18] microwave properties of various Zingiberaceace family plants are presented at 2.45GHz using a substrate integrated cavity. Microwave methods are based on the measurement of the dielectric properties of the sample under test (SUT). DPs refer to both real and imaginary parts of the permittivity, known as dielectric constant (ϵ') and dielectric loss factor (ϵ'') as follows:

$$\epsilon = \epsilon' - j\epsilon'' \tag{1}$$

Physically, ϵ' is related to the ability of the material to store energy, while ϵ'' is related to the conversion of electromagnetic energy into heat, with j being the imaginary term. Permittivity can be affected by diverse factors associated with the nature of the material, therefore it is susceptible to changes if the sample is adulterated.

Measurements of dielectric properties can be divided in resonant and non-resonant methods; however, resonant methods offer greater accuracy but they are limited to only a single frequency [19].

Several papers have addressed the usage of resonant methods to detect adulteration. In [20], adulteration detection of liquid silicone is presented using metamaterial inspired resonators, where the samples are adulterated with different types of oils. In [21], a high impedance surface electromagnetic bandgap resonator is used to measure different degrees of adulteration of fish oil with olive oil. Moreover, in [22] several food flours are adulterated and measured using a miniaturized electric LC resonator.

In all the above mentioned works, the adulterant is always a single component added to the sample under test (SUT), therefore, clear regression trends are found between adulterant percentage and and resonant frequency.

In this paper, we propose to characterize turmeric samples contaminated with two of the most common adulterants: corn starch and yellow dye [15] using the Cavity Perturbation Technique (CPT) [23]. We employ a cylindrical cavity excited at one of the Federal Communications Commission (FCC) allocated frequencies for industrial, scientific, and medical purposes (2.4GHz) in the TE_{111} fundamental mode [24]. The choice of the cavity is related to its intrinsically high Q value [25], however, any resonator based on perturbation theory [26], [27], [28], [29], [30] could have been utilized as well.

By using the CPT, clear trends in resonant frequency and Q values vs. adulteration percentage are obtained for a single adulterant. However, when two contaminants are added, conventional CPT analysis cannot predict adulteration. For this reason we use machine learning techniques based on hardware-aware predictive model optimization that are able to detect the adulteration contents for all scenarios with higher confidence levels.

The availability of large complex data sets combined with killer applications has made Artificial Intelligence (AI) one of the most exciting and promising new technologies. Machine learning itself is a form of artificial intelligence (AI) that can execute tasks without being explicitly programed [31]. Instead, it learns from a training set so that it can execute the tasks on any new data. This is particularly useful for applications in which the data is difficult to model analytically. Training the predictive model requires learning a set of coefficients (weights) from the training data. When the training data is labelled, it is referred to as supervised learning, which is currently the most widely used approach, and what we will cover in this work. Inference involves performing a given task using the learned coefficients.

Recent surveys have listed a variety of different machine learning techniques applied to inspect the quality of fruits and vegetables [32], [33], [34]. In our work, we investigate the use of machine learning techniques to detect the type and amount of turmeric adulterants by analyzing the dielectric properties, and address several issues that have still not been addressed when using machine learning for these types of applications. First, often the predictive model with highest accuracy is used although this might be the most computationally intensive that also consumes the most power. For battery operated embedded systems this approach is not the most realistic. Second, the predictive model is normally not further optimized, and especially not considering the underlying hardware platform on which it will be executed.

To address these issues, in this work we present a fully automated flow that generates an optimized predictive model based on the target hardware platform, e.g., FPGA, ASIC, GPU or micro-controller. Due to its importance, we apply this flow to improve the purity measurement of turmeric. In summary the main contributions of this work are:

1) Microwave characterization of turmeric adulterated with two of the main adulterants at different ratios (starch and color) using Cavity Perturbation Technique (CPT) at 2.4GHz.
2) Propose a fully automated flow that can generate an optimized predictive model taking into consideration the target HW platform.
3) Perform extensive results showing that CPT alone cannot detect the adulteration contents and showing the effectiveness of our predictive model optimization flow for different hardware platforms.

II. RELATED MACHINE LEARNING WORK

Many applications from different domains have been shown to benefit from machine learning. These areas include video (arguably the biggest source of data) [35], speech recognition [36], and medical applications [37], [38].

Much work in the area of efficient machine learning deals with image processing due to its importance [35], [39]. Because of this, extensive effort has been done to automate the design and optimization of neural networks for image processing [40].

Machine learning has also been used in the food industry mainly to inspect the quality of produce. In [32] the authors survey previous work that has been proposed to examine the

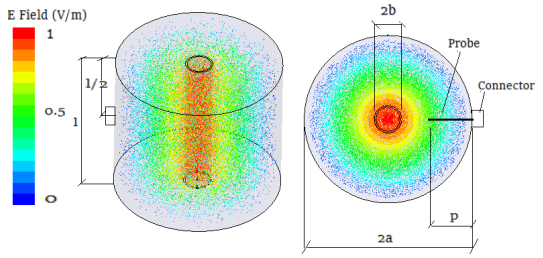

FIGURE 1. Cavity simulation result.

quality of fruits and vegetables. Zhou et al. discussed in [33] the use of deep learning for food recognition, and quality detection of fruits, vegetables, meat and aquatic products. In [34] the authors review application of machine learning algorithms that use low frequency properties in quality assurance of black tea.

Closer to our work, recent advances on hardware-aware modeling and optimization for ML applications have emerged [41], [42], again mainly in the area of image processing through deep neural networks (DNNs).

To the best of our knowledge this is the first work that optimizes predictive models based on different target hardware platforms and that does technology independent as well as technology dependent model optimizations. To demonstrate the robustness of our proposed flow we investigate the use of machine learning techniques to detect the type and amount of turmeric adulterants by analyzing the dielectric properties, showing that only looking at these properties does not lead to results that are accurate enough.

III. DIELECTRIC PROPERTIES ANALYSIS AND SETUP

The dimensions of the cavity are a = 4.9 cm and l = 8.6 cm, calculated from equation 2.

The cavity is simulated using HFSS and the E-field is shown in Fig. 1, where it is clear that for the TE_{111} mode, the E-field is concentrated at the center of the cavity, where the sample holder should be placed for highest sensitivity.

The cavity is machined in aluminum. To excite the TE_{111} mode, an electrical probe-coupling is desired; therefore, an SMA connector is placed at the center of the cavity and its center conductor extended experimentally to a length p=35 mm where the maximum coupling is achieved (Fig. 1).

The dielectric measurements were performed using the Cavity Perturbation Technique (CPT) by connecting a cylindrical cavity to a vector network analyzer (VNA) (Agilent 8510) as depicted in figure 2. The VNA is set to measure from 1900 MHz to 2400 MHz with 401 points. The cavity is designed to operate at 2.4GHz in the TE_{111} mode. The measured cavity unloaded Q is Q_0=2550 without sample holder.

$$f_1 = \frac{c}{2\pi\sqrt{\mu'\epsilon'}}\sqrt{\left(\frac{\rho'_{pm}}{a}\right) + \left(\frac{\rho\pi}{l}\right)^2} \tag{2}$$

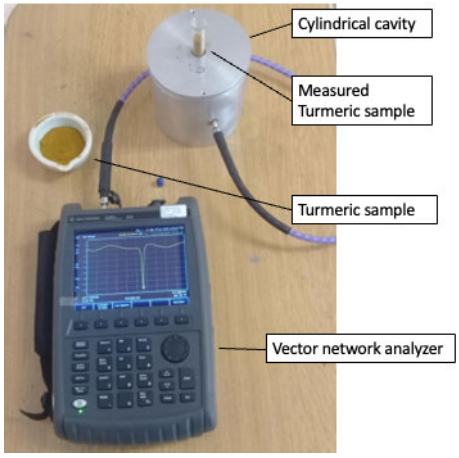

FIGURE 2. Measurement setup overview based on Cavity Perturbation Technique (CPT) connected to vector network analyzer.

where a is the radius, l is the length, c is the speed of light; n, m, and p are the subscripts of the propagation modes; μ' is the magnetic permeability, and ρ_{nm}' is the root of the derivative of Bessel's function.

The CPT method is described by equations 3 and 4 as follows:

$$\frac{f_1 - f_2}{f_2} = A\left(\epsilon'_r - 1\right)\frac{V_s}{V_c} \tag{3}$$

$$\frac{1}{Q_2} - \frac{1}{Q_1} = B\epsilon''_r\frac{V_s}{V_c} \tag{4}$$

where f_1 and f_2 are the frequencies before and after perturbation. V_s and V_c are the volumes of the sample and cavity respectively; and Q_2 and Q_1 are the quality factors after and before perturbation. A and B are constants that requires an initial calibration. For this we use olive oil as suggested in [43].

Moreover, in order to extract the particle permittivity, the Landau & Lifshitz, Looyenga (LLL) equation was utilized shown in equation 5 [44]. In particular:

$$\epsilon_{part} = \left[\frac{\epsilon_{bulk}^{1/3} + v_s - 1}{v_s}\right]^3 \tag{5}$$

where ϵ_{part} is the particle permittivity, ϵ_{bulk} is the permittivity of the mixture (air-particle) and with $v_s = \rho_{bulk}/\rho_{part}$, where ρ_{bulk} is the bulk density and ρ_{part} is the particle density.

In order to calculate the bulk densities, 25ml of the sample were poured in a graduated beaker (100ml ± 1ml). Then the sample was weighed with an electronic scale. The particle density was measured by the water displacement method.

All measured results were analyzed by ANOVA and Tukey's pairwise comparisons at a significant level of r<0.05 using Matlab 17.

IV. PREDICTIVE MODEL GENERATION

This section describes in detail how we use machine learning to increase the accuracy of the adulteration prediction.

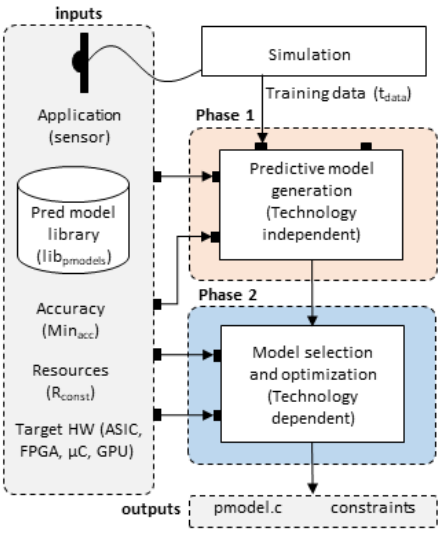

FIGURE 3. Overview of complete predictive model generation flow proposed flow composed of two phases. Phase 1: Predictive model generation. Phase 2: Model selection and optimization.

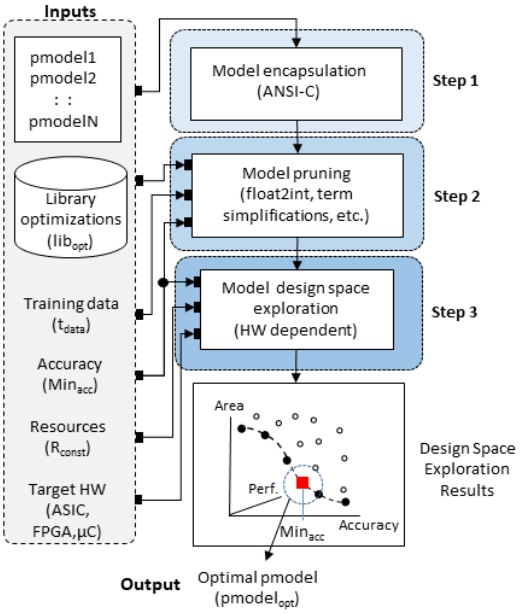

FIGURE 4. Phase 2: Overview of the predictive model generation and optimization phase composed of 3 steps. Step 1: Model encapsulation. Step 2: Model pruning. Step 3: Model exploration.

Training the predictive model requires learning a set of coefficients (weights) from the training data. When the training data is labeled, it is referred to as supervised learning, which is currently the most widely used approach, and what we use in this work. Inference involves performing a given task using the learned coefficients. Using this principle, we use machine learning to improve the dielectric properties sensing for turmeric adulteration detection.

Fig. 3 shows an overview of our complete automated flow. The flow takes as input the application that needs the predictive model. The flow also takes a library of predictive models (lib_{models}), the minimum requires accuracy of the model (min_{acc}), the target HW platform (e.g., ASIC, FPGA, or micro-controller) and any resource constraints, e.g., number of HW multipliers available or amount memory. The output is a compiled (for SW) or synthesized (for HW) predictive model on the target HW platform.

The flow itself is composed of two phases. Phase 1 generates different predictive models. The models that meet the required minimum accuracy is then passed to phase 2 where the models are optimized based on the HW platform and the most efficient model selected. The next subsection describes these three phases in detail.

Phase 1: Predictive Model Generation: This first phase takes as input the training data obtained from simulation, a minimum required accuracy (min_{acc}) and trains different predictive models given from a library of predictive models (lib_{pred}). For this we use scikit-learn [45]. The idea is to generate a variety of different predictive model with the required minimum accuracy such that the next phase can then optimize the models and find the most optimal for the given HW platform. Some of the predictive models used include liner regression (LR), regression trees (LT), multi-level perceptron (MLP) and support vector machine (SVM) models.

It should be noted that the quality of the predictive model depends on the training data. To investigate the effectiveness of our predictive model we first rely on the simulation data, while later make use of the measurement data. A 10-fold cross validation is used to measure the accuracy of the model, where the training data is split into 10 regions and 9 are used for training and 1 for testing consecutively.

Phase 2: Model Selection and Optimization: This second phase takes as input the predictive models generated in phase 2 and optimizes them in order to find the fastest, smallest (area or code size) and/or lowest power depending on the target HW platform. This phase can be further sub-divided into three steps as shown in Fig. 4.

Step 1 takes as input the different predictive models and converts them into ANSI-C. The main reason for this is that ANSI-C can easily be re-targeted to the different HW platforms supported by our flow. Compiling ANSI-C with any cross-compiler enables running the predictive model on any processor, while using High-Level Synthesis (HLS) enables a path to synthesize the ANSI-C code into RTL (Verilog or VHDL) so that the model can be instantiated as a dedicated HW module in an ASIC or FPGA.

Step 2 takes the predictive models as input and applies different optimization on them in order to simplify each model as much as possible within Min_{acc}. As shown in Fig. 4, different predictive model optimizations are used given in an optimization library. These include, floating point to fixed point data conversion and predictive model terms pruning. These optimizations are greedily applied starting by the floating point to fixed point conversion, followed by the term pruning optimization. This eliminates any terms in the model that have small coefficients, e.g., in the MLP case

the neurons with smallest weights. After each pruning, the predictive model is re-simulated and the accuracy measured. This process is repeated until the minimum allowable accuracy (Min_{acc}) is reached.

Step 3 takes as input the optimized predictive models and performs a technology dependent design space exploration in order to obtain the most efficient implementation for each predictive model. In the case of targeting an ASIC of FPGA, HLS has the ability of generating a variety of different HW implementations mainly by specifying synthesis directives in the form of pragmas into the C code. These directives control how to synthesize arrays (e.g., RAM or registers), loops (fully unroll, partially unroll, not unroll or pipeline) and functions (e.g., inline or not). As shown in Fig. 4, different combinations of these pragmas lead to designs with unique trade-offs. In this case, area, and performance and accuracies. Out of all the combinations the most important ones are the ones that lead to the Pareto-optimal designs, highlighted as black circles in the trade-off curve). HLS DSE is a typical multi-objective optimization problem [46]. In traditional HLS DSE the main goal is to find all the Pareto-optimal designs quickly. In this particular work, our goal is simply to find the smallest design, with the minimum required accuracy, that does not exceed the maximum resource constraint given by the user (R_{const}), if any. One approach would be to exhaustively enumerate all possible pragma combinations and invoke the HLS process for each combination and then return the design implementation that leads to the best results based on the constraints set. This has the advantages of leading to the optimal solution as all possible combinations are tried, but the obvious drawback of potentially requiring a long time as the search space grows supra-linearly with the number of explorable operations (arrays, loops and functions). Thus, faster methods are required.

In this case, for predictive models with large search spaces, we use a genetic algorithm (GA) where each explorable operation is equivalent to a chromosome Cr. This Cr is then combined and mutated based on pre-defined crossover and mutation probabilities (pc and pm) to produce an offspring. Thus, the explorer starts by generating two parents with random Cr and synthesizing these in order to obtain their area and performance. The cost of each parent can in turn be computed from this. Given the mutation and crossover rate, an offspring with a unique set of attributes is generated, and the explorer synthesizes it. The explorer then continues by comparing the result of the child vs. its parents and substituting one of them in case that any of the child has a lower cost. This process is repeated until no child can improve the cost function for N iterations, where N is a GA specific hyper-parameter which in our case is set to 10 as suggested by [47].

In the case that the target HW platform is a microprocessor or micro-controller, instead of synthesis directives, our flow explores different compiler options (e.g., -01, -02, -03). In this case an exhaustive enumeration of all compiler options is enough as the search space is much smaller than for the HLS case.

After all the explorations of all the valid and optimized predictive models, our flow selects the smallest model that meets the given constraints. The output of this phase is the the ANSI-C description of the most optimized model and the compiler or HLS synthesis option that will generate the optimized model for the target HW platform.

Finally, the predictive model based on the selected hardware platform is deployed. In the case that the model must run on a microprocessor or micro-controller then it will be compiled, while in the case of having to build a dedicated hardware module (e.g., ASIC and FPGA), then the predictive model is synthesized using HLS into RTL (Verilog or VHDL) and this in turn synthesized (logic synthesis) into a gate netlist.

TABLE 1. Nutritional value comparison between Turmeric and Corn starch.

Information per 100g	Turmeric [g]	Corn starch [g]
Proteins	8	0.4
Total fats	10	0.2
Saturated fats	3.1	0
Polyunsaturated fats	.0022	0
Mono unsaturated fats	1.7	0
Carbohydrates	65	86.4
Sugars	3.2	0
Fiber	21	0.1
Sodium	38	0.0025
Cholesterol	0	-
Potassium	0.0025	-

V. EXPERIMENTAL EVALUATION

This section measures the effectiveness of our proposed method. Initially the experimental setup is described in detail, followed by the experimental results and their discussion.

A. EXPERIMENTAL SETUP

Organic turmeric and corn starch were purchased at a local supermarket, the nutritional information as per the manufacturer is shown in table 1. Egg yellow edible color in powder consisting of Sodium chloride, tartrazine (E102) and orange color A1 (E110) was also acquired at a local supermarket and used as contaminant.

Before connecting the cavity to the VNA, a standard open-short-load calibration is performed to remove the cable effects. A sample holder is added to the cavity and an epoxy ring of about 1 cm radius was glued at the bottom. The measured unloaded Q value with an empty sample holder is $Q_1 = 923$ at a resonant frequency of $f_1 = 2244$MHz. To obtain A and B, a volume (Vs=10ml) of olive oil is added to the sample holder. The recorded values are: Resonant frequency f_2=2156 and Q_2=85. By taking the permittivity values as ϵ'=3 and ϵ''=0.035 for olive oil [43]. and solving equations 3 and 4, we get A=0.76 and B=0.05.

Turmeric samples were adulterated with **egg yellow** color at different concentrations as shown in table 2. Table 3 shows

TABLE 2. Adulteration of Turmeric with Color (r<0.05).

Ratio Turmeric[g]:Color[g]	f_0 [MHz]	Q_0	ϵ_{Bulk}'	ϵ_{Bulk}"	ϵ_{part}'	ϵ_{part}"
10:0	2171	85.8	2.5	0.031	4.4	0.080
10:1	2161	80.8	2.7	0.033	4.8	0.086
10:3	2158	74.3	2.7	0.036	4.7	0.090
10:6	2152	78.1	2.8	0.034	4.8	0.080
10:10	2151	94.3	2.9	0.028	4.9	0.065
0:10	2131	440.7	3.3	0.004	5.4	0.006

TABLE 3. Adulteration of Turmeric with Starch (r<0.05).

Ratio Turmeric[g]:Starch[g]	f_0 [MHz]	Q_0	ϵ_{Bulk}'	ϵ_{Bulk}"	ϵ_{part}'	ϵ_{part}"
10:0	2170	87.2	2.52	0.030	4.4	0.08
10:1	2173	89.5	2.47	0.029	4.6	0.083
10:3	2173	94.7	2.47	0.028	5.0	0.09
10:6	2177	97.5	2.37	0.027	5.2	0.10
10:10	2180	84.5	2.32	0.031	5.6	0.13
0:10	2190	102.9	2.10	0.025	8.0	0.21

how the Turmeric sample was adulterated with different starch concentrations. The mixture was homogenized by hand stirring and 11g were added to the the sample holder. All measurements were taken by triplicate.

To test our complete flow, we apply the proposed predictive model approach to detect impurities in turmeric as presented in the introduction. For this, the data obtained from the sensor's measurements are used to build the initial predictive model that detects the contamination amount using a library of predictive models using scikit-learn [45].

To show the effectiveness of our proposed approach, we target two different platforms. The first is a low-cost microcontroller. In particular, TI's MSP430, which contains a 16-bit CPU [48]. Code composer studio 9.3.0 is used as the compiler [49]. The second case is a 45nm ASIC (Nangate Open cell) using HLS with target a synthesis frequency of 200MHz. The HLS tool used for this purpose is NEC CyberWorkBench [50]. This should allow us to fully characterize our proposed method in terms of instruction reductions in the software case and area reduction in the hardware case.

B. EXPERIMENTAL RESULTS

First, we will present the results of how our microwave measuring setup is able to generate the data that we will then feed to our predictive model estimation flow. The results also motivate the need to use a predictive model.

1) RESULTS FOR COLOR CONTAMINATION

Figure 5 shows the averaged reflection coefficient (S11) at different adulteration levels (r<0.05). Figure 6a shows the resonant frequency f_o vs. the percentage of turmeric in the mixture. In order to describe the relationship between f_o and turmeric amount, a regression model was calculated using MATLAB [51].

As it can be seen, the resonant frequency decreases linearly as a function of added color as shown by the regression

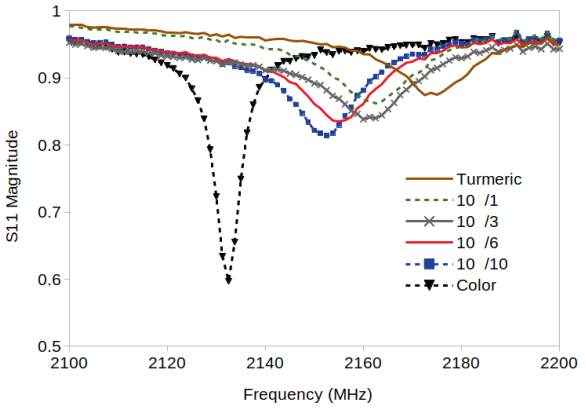

FIGURE 5. Averaged S11 response for different color adulteration levels.

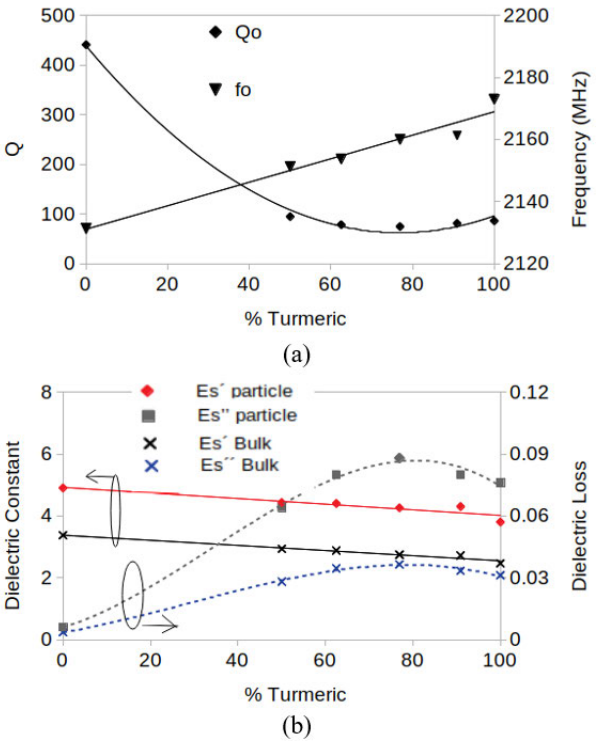

FIGURE 6. Frequency response for color adulteration. (a) Resonant frequency vs. turmeric+color mixture. (b) Dielectric constant and loss vs. turmeric+color mixtures.

equation 6 with a correlation coefficient R^2=0.9616. The maximum resonant frequency is obtained for 100% Curcuma (fo=2171MHz). And the minimum for 100% color (2,131 MHz).

$$f_o(\%turmeric) = 37.8(\%turmeric) + 2131 \quad (6)$$

For the unloaded quality factor, the trend line follows the polynomial given by equation 7 (R^2=0.9953), where a minimum value of Qo is obtained at 77% turmeric (Qo=74.3), for higher turmeric concentrations the Qo value increases slightly to 85.8 for 100% turmeric. For lower than 77% turmeric concentration, Qo increases, reaching a maximum

of 440.7 when we have 100% color.

$$Qo(\%turmeric) = 0.0637(\%turmeric)^2 - 9.79(\%turmeric) + 438 \quad (7)$$

Figure 6b shows the bulk permittivity value extracted with the CPT, equations 3 and 4. It is observed that ϵ_{bulk}' decreases linearly as turmeric concentration increases (equation 8) (R^2=0.9630), from about 3.3 for 0% turmeric to about 2.5 for 0% turmeric. The imaginary part (ϵ''_{bulk}) shows an inverted U behavior (equation 9) (R^2=0.9955), having a maximum for 77% turmeric (0.036). For 0% turmeric we reach a minimum of 0.0035 and for 100% turmeric we have 0.031.

$$\epsilon'_{bulk}(\%turmeric) = -0.0082(\%turmeric) + 3.37 \quad (8)$$

$$\epsilon''_{bulk}(\%turmeric) = -7.48 \times 10^{-8}(\%turmeric)^3 + 6.5 \times 10^{-6}(\%turmeric)^2 + 0.00036 \times (\%turmeric) + 0.003 \quad (9)$$

In order to calculate the particle permittivity equation 5 was utilized. The bulk and particle densities were extracted as explained in the previous section, obtaining the following values: bulk density of turmeric ρ_{bulk}=0.53 g/ml; particle density of turmeric ρ_{part}=0.96 g/ml; color bulk density ρ_{bulk}=1.3 g/ml; and color particle density ρ_{part}=2 g/ml.

Figure 6b shows the real part of the permittivity ($\epsilon_{part}{}'$), where a linear correlation exists (equation 10) (R^2=0.8519). The maximum is for 0% turmeric (5.4) and the minimum for 100% turmeric (4.4). For the imaginary part ($\epsilon_{part}{}''$), the inverted U trend continues (equation 11) (R^2=0.995), with a maximum for 77% turmeric of 0.09 and a minimum for 0% turmeric of 0.006. For 100% turmeric we have 0.08.

$$\epsilon'_{part}(\%turmeric) = -0.009(\%turmeric) + 4.9 \quad (10)$$

$$\epsilon''_{part}(\%turmeric) = -2.1 \times 10^{-7}(\%turmeric)^3 + 2.1 \times 10^{-5}(\%turmeric)^2 + 0.00064 \times (\%turmeric) + 0.006 \quad (11)$$

2) RESULTS FOR STARCH CONTAMINATION

The same experiments where repeated using starch at different concentrations (Table 3). Figure 7 presents the S11 response (r<0.05) where it is seen that the resonant frequency (Figure 8a) has a linear relationship to adulterant content (12)(R^2=0.984). The largest f_o (2190MHz) is achieved for 0% turmeric and the lowest f_o (2170) for 100% turmeric.

For the unloaded Q (Qo) more starch implies higher Qo. The trend exhibits a linear behavior (equation 13) (R^2=0.418) where the largest value is Qo=102.9 for 0% turmeric, and 100% turmeric it reduces to 87.2.

$$fo(\%turmeric) = -20(\%turmeric) + 2179 \quad (12)$$

$$Qo(\%turmeric) = -12.36(\%turmeric) + 100.2 \quad (13)$$

Regarding the bulk dielectric constant (Figure 8(b)) we have a linear trend (equation 14) (R^2=0.984) and (equation 15) (R^2=0.366), with a slightly decreasing value

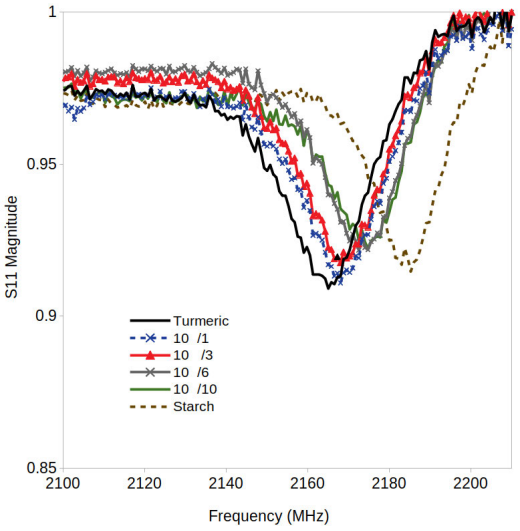

FIGURE 7. Averaged S11 response for different starch adulteration levels.

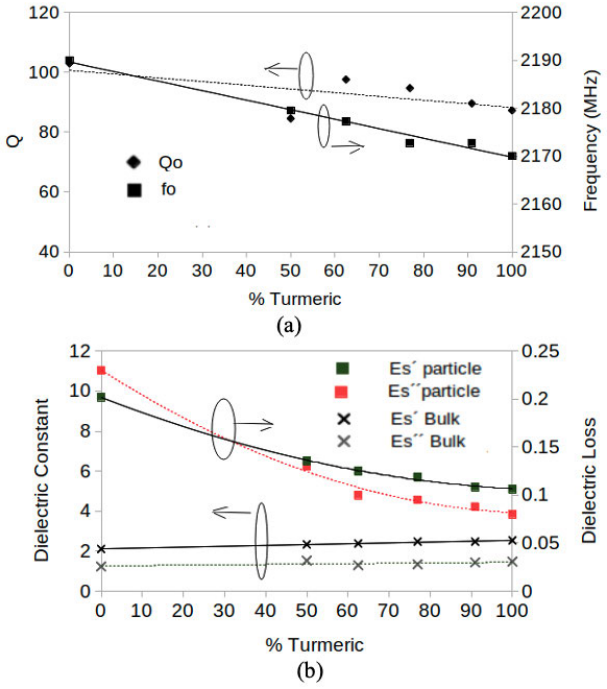

FIGURE 8. Frequency response for starch adulteration. (a) Resonant frequency vs. turmeric+starch mixture. (b) Dielectric constant and loss vs. tumeric+starch mixtures.

for larger starch content (for both, $\epsilon_{bulk}{}'$ and $\epsilon_{bulk}{}''$). For the real part, a maximum of $\epsilon_{bulk}{}'$=2.52 is recorded for 0% starch and a minimum of 2.1 for 100% starch. For the dielectric loss we have 0.030 for 0% starch, with a decreasing trend to 0.025 for 100% starch as shown in Figure 8(b).

$$\epsilon'_{bulk}(\%turmeric) = 0.004(\%turmeric) + 2.32 \quad (14)$$

$$\epsilon''_{bulk}(\%turmeric) = 0.00004(\%turmeric) + 0.026 \quad (15)$$

By calculating the particle dielectric constant we obtain a polynomial trend (equation 16) (R^2=0.998), where the maximum of the real part is achieved for 100% starch (equation 8)

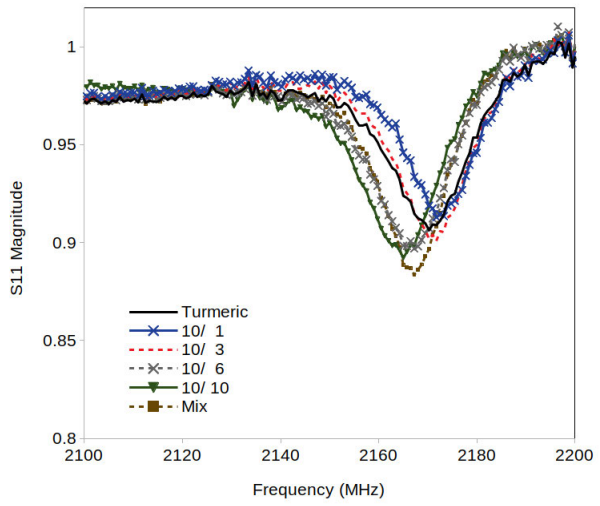

FIGURE 9. Averaged S11 response for different color+starch adulteration levels.

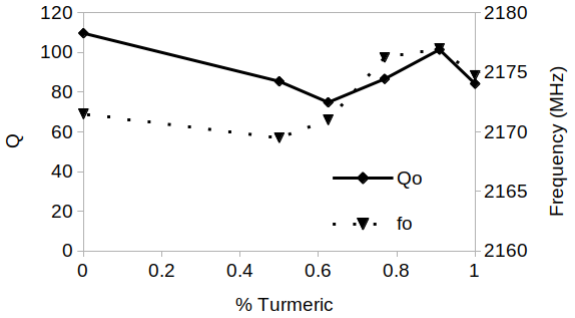

FIGURE 10. Q and f_o for different color+starch adulteration levels.

and a minimum for 0% starch (4.4). Similarly, for the loss we also have a polynomial trend (equation 17) (R^2=0.993). ϵ_{bulk} is 0.21 for 100% starch and a minimum $\epsilon_{bulk}{}'$=0.08 for 0% starch.

$$\epsilon'_{part}(\%turmeric) = 0.00034(\%turmeric)^2 + 0.08(\%turmeric) + 9.7 \quad (16)$$

$$\epsilon''_{part}(\%turmeric) = -1.26 \times 10^{-5}(\%turmeric)^2 + 0.0027(\%turmeric) + 0.23 \quad (17)$$

In both previous cases (turmeric with color and starch) it is clear that we can find behavioral trends using regression models in both f_o and Qo, making it possible to predict adulteration. However, when we try a mix of 50% color / 50% starch the regression analysis does not show a clear trend as shown in Figure 9 and Figure 10 (r<0.05). For the fo, the overall change in resonant frequency varies only 4MHz for the whole range (from 0 turmeric to 100 turmeric), compared to 40MHz in the color case and 20MHz in the starch case. Moreover, the trend shows an undulatory behavior, similarly for the Qo, making a regression analysis difficult. For this reason, in order to predict adulteration, we will employ a machine learning method, where the S11 data from starch and color adulteration will be used for the training algorithm.

3) PREDICTIVE MODEL RESULTS

To test our proposed flow, we apply the proposed machine learning approach to detect impurities in turmeric as presented in the introduction.

The data obtained from the sensor's measurements is used to build the initial predictive model that detects the contamination amount using a library of predictive models using scikit-learn [45].

To show the effectiveness of our proposed approach, we target two different platforms. The first is a low-cost microcontroller. In particular, TI's MSP430, which contains a 16-bit CPU [48]. Code composer studio 9.3.0 is used as the compiler [49]. The second case is a 45nm ASIC (Nangate Open cell) using HLS with target a synthesis frequency of 200MHz. The HLS tool used for this purpose is NEC CyberWorkBench [50]. This should allow us to fully characterize our proposed method in terms of instruction reductions in the software case and area reduction in the hardware case..

In both cases the Support Vector Machine (SVM) model was found to be the most accurate predictive model from the library of predictive models investigated. SVM could achieve a prediction accuracy of 99%. Unfortunately, SVM is also the most computationally intensive model. Thus, we also investigated if relaxing the precision accuracy could lead to other, less computationally intensive models, to become viable.Table 4 shows the results, which depicts the predictive model with lowest computationally complexity for different precision accuracy.

For the ASIC case our proposed exploration framework is executed using an exhaustive enumeration of all synthesis directives and using the proposed genetic algorithm (GA). For the micro-controller case an exhaustive enumeration of all the compiler options was enough as the search space is much smaller.

TABLE 4. Overview of smallest predictive models used for different accuracies and hardware platforms.

Accuracy [%]	ASIC	Microcontroller
99	SVM	SVM
95	SVM	SVM
90	MLP	REPtree
85	LR	LR

Fig. 11, Fig. 12 and table 4 summarize the results in terms of area and code reduction for the ASIC and micro-controller cases respectively when the minimum required accuracy of the model is relaxed from 99% to 85%, and taking the original predictive model obtained after phase 1 as reference (100% area and code size). From the results we can make the following observations:

Observation 1: From table 4 we can see that when the prediction accuracy is relaxed different simpler predictive models are now better. The table also shows that the best

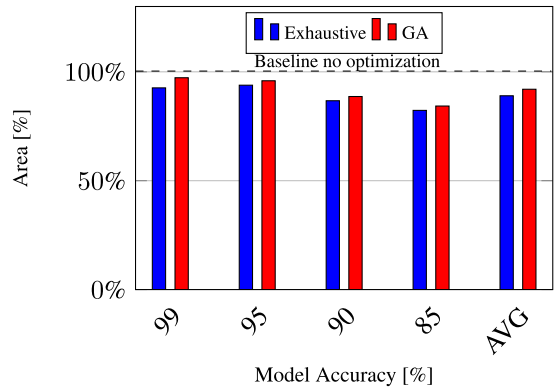

FIGURE 11. Area reduction of proposed flow targeting an ASIC. Exhaustive technology dependent search vs. genetic algorithm.

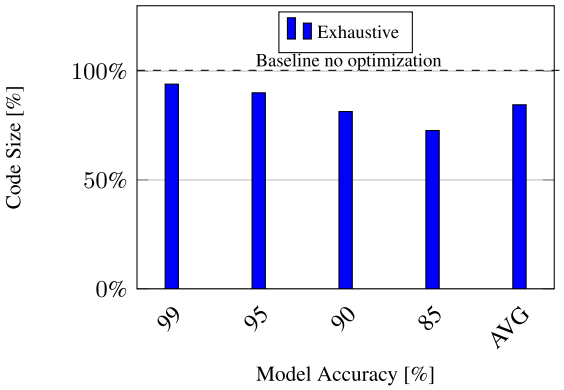

FIGURE 12. Code reduction of proposed flow targeting TI MSP430 micro-controller.

predictive model is not the same for different hardware platforms, and hence, it further strengthens our view of the need of having technology dependent model selection and optimization.

Observation 2: In both cases, our proposed method was able to further optimize the predictive model for this case study. In particular, on average, the area was reduced by 10% and up to 16% for the ASIC case and on average 14% and up to 24% for the micro-controller case.

Observation 3: Larger savings are obtained when the minimum allowable accuracy is relaxed. There are two reasons for this. First, our optimization phase can more aggressively optimize the predictive model. Second, a smaller and more efficient predictive model can now be used. As shown in table 4, in both cases (ASIC and micro-controller), a different predictive model is used when the accuracy is relaxed to 90%. In the ASIC case from SVM to MLP and in the micro-controller case from SVM to REPtree.

Observation 4: When capturing real data and re-analyzing it, we noticed that the accuracy of the predictive models on average was reduced by 5%. Adding the new training data and re-calibrating the predictive models allowed our flow to bring back the accuracy to the desired minimum accuracy.

Observation 5: The proposed genetic algorithm (GA) based search leads to similar results (on average 3% worse) than the exhaustive search while being on average 22× faster.

In summary, based on these results we can conclude that our proposed fully automated results is very effective at finding and optimizing predictive model for different hardware platforms.

VI. SUMMARY AND CONCLUSION

This paper successfully presents a method to detect turmeric adulteration using the Cavity Perturbation Technique (CPT) at 2.4GHz. Two different adulterants are examined (egg-yellow color and starch).

It is shown that as color is added, the resonant frequency decreases linearly as a function of added color. For the unloaded quality factor, a polynomial trend is found, where a minimum value of Qo is obtained at 77% turmeric, and maximum is seen for 100% color. Moreover, ϵ' has a linear relationship to color, whereas ϵ'' exhibits an inverted U behavior. When turmeric is adulterated with starch it is seen that the resonant frequency has a linear relationship to adulterant content. For Qo, more starch results in higher Qo in a linear trend. ϵ' exhibits a polynomial tendency with a maximum for 0% turmeric and ϵ'' presents a linear behavior.

We have also shown that when turmeric was adulterated with different concentrations of the two adulterants (e.g., a 50% color/50% starch), no clear trend was observed by analyzing f_o and Qo, making it unfeasible to identify adulteration. However, by applying Machine Learning and training it with raw S11 data, contamination identification was possible with high accuracy. In particular we show that the accuracy of our predictive model depends on the complexity of the model and hence impacting the code size or silicon area of the model depending on where the predictive model is implemented. We have also shown the smallest predictive model is also platform dependent and that it also depends on the minimum required accuracy. Based on this we have proposed an automated hardware dependent predictive model explorer.

REFERENCES

[1] S. Dhakal, K. Chao, W. Schmidt, J. Qin, M. Kim, and D. Chan, "Evaluation of turmeric powder adulterated with metanil yellow using FT-Raman and FT-IR spectroscopy," *Foods*, vol. 5, no. 4, p. 36, May 2016.
[2] N. Hishikawa, Y. Takahashi, Y. Amakusa, Y. Tanno, Y. Tuji, H. Niwa, N. Murakami, and U. Krishna, "Effects of turmeric on Alzheimer's disease with behavioral and psychological symptoms of dementia," *AYU Int. Quart. J. Res. Ayurveda*, vol. 33, no. 4, pp. 499–504, 2012.
[3] J. W. Daily, M. Yang, and S. Park, "Efficacy of turmeric extracts and curcumin for alleviating the symptoms of joint arthritis: A systematic review and meta-analysis of randomized clinical trials," *J. Medicinal Food*, vol. 19, no. 8, pp. 717–729, Aug. 2016.
[4] I. Chattopadhyay, K. Biswas, U. Bandyopadhyay, and R. K. Banerjee, "Turmeric and curcumin: Biological actions and medicinal applications," *Current Sci.*, vol. 87, no. 1, pp. 44–53, 2004.
[5] Y. G. Lin, "Curcumin inhibits tumor growth and angiogenesis in ovarian carcinoma by targeting the nuclear factor-kappaB pathway," *Clin. Cancer Res.*, vol. 13, pp. 3423–3430, Jun. 2007.
[6] A. G. Osman, V. Raman, S. Haider, Z. Ali, A. G. Chittiboyina, and I. A. Khan, "Overview of analytical tools for the identification of adulterants in commonly traded herbs and spices," *J. AOAC Int.*, vol. 102, no. 2, pp. 376–385, Mar. 2019.

[7] A. Girme, G. Saste, A. K. Balasubramaniam, S. Pawar, C. Ghule, and L. Hingorani, "Assessment of curcuma longa extract for adulteration with synthetic curcumin by analytical investigations," *J. Pharmaceutical Biomed. Anal.*, vol. 191, Nov. 2020, Art. no. 113603.

[8] V. A. Parvathy, V. P. Swetha, T. E. Sheeja, and B. Sasikumar, "Detection of plant-based adulterants in turmeric powder using DNA barcoding," *Pharmaceutical Biol.*, vol. 53, no. 12, pp. 1774–1779, Dec. 2015.

[9] K. Dhanya and B. Sasikumar, "Molecular marker based adulteration detection in traded food and agricultural commodities of plant origin with special reference to spices," *Current Trends Biotechnol. Pharmacy*, vol. 4, no. 1, pp. 454–489, 2010.

[10] A. Di Maro, E. K. Essuman, E. Teye, R. G. Dadzie, and L. K. Sam-Amoah, "Consumers' knowledge of food adulteration and commonly used methods of detection," *J. Food Qual.*, vol. 2022, Apr. 2022, Art. no. 2421050.

[11] A. R. Sen, P. S. Gupta, and N. G. Dastidar, "Detection of curcuma zedoaria and curcuma aromatica in curcuma longa(turmeric) by thin-layer chromatography," *Analyst*, vol. 99, no. 1176, pp. 153–155, 1974.

[12] A. Booker, D. Frommenwiler, D. Johnston, C. Umealajekwu, E. Reich, and M. Heinrich, "Chemical variability along the value chains of turmeric (curcuma longa): A comparison of nuclear magnetic resonance spectroscopy and high performance thin layer chromatography," *J. Ethnopharmacology*, vol. 152, no. 2, pp. 292–301, Mar. 2014.

[13] B. Sasikumar, S. Syamkumar, R. Remya, and T. John Zachariah, "PCR based detection of adulteration in the market samples of turmeric powder," *Food Biotechnol.*, vol. 18, no. 3, pp. 299–306, Jan. 2004.

[14] S. Kar, B. Tudu, A. Jana, and R. Bandyopadhyay, "FT-NIR spectroscopy coupled with multivariate analysis for detection of starch adulteration in turmeric powder," *Food Addit Contaminants, A*, vol. 36, no. 6, pp. 863–875, Jun. 2019.

[15] R. Ranjan, N. Kumar, A. H. Kiranmayee, and P. C. Panchariya, "Application of handheld NIR spectroscopy for detection of adulteration in turmeric powder," in *Proc. 7th Int. Conf. Adv. Comput. Commun. Syst. (ICACCS)*, vol. 1, Mar. 2021, pp. 1238–1241.

[16] V. J. Murthy, N. S. Kiranmai, and S. Kumar, "Study of dielectric properties of adulterated milk concentration and freshness," *IOP Conf. Ser., Mater. Sci. Eng.*, vol. 225, Aug. 2017, Art. no. 012285.

[17] A. Aziz, J. Hassan, K. Khalid, and Z. Abbas, "Microwave dielectric characterization of turmeric," *Solid State Sci. Technol.*, vol. 19, no. 1, pp. 206–211, 2019.

[18] N. A. Abd. Aziz, J. Hassan, Z. Abbas, and N. H. Osman, "Microwave dielectric properties of four types of rhizomes from zingiberaceace family," *J. Phys. Sci.*, vol. 28, no. 1, pp. 15–26, 2017.

[19] J. Krupka, "Frequency domain complex permittivity measurements at microwave frequencies," *Meas. Sci. Technol.*, vol. 17, no. 6, pp. R55–R70, Apr. 2006.

[20] N. K. Tiwari, P. K. Varshney, D. Mondal, and M. J. Akhtar, "Rf sensor for adulteration detection of liquid silicone used in medical industry," in *Proc. 18th Medit. Microw. Symp. (MMS)*, 2018, pp. 313–316.

[21] R. Yadav and P. N. Patel, "Experimental study of adulteration detection in fish oil using novel PDMS cavity bonded EBG inspired patch sensor," *IEEE Sensors J.*, vol. 16, no. 11, pp. 4354–4361, Jun. 2016.

[22] P. K. Varshney, A. Sharma, and M. J. Akhtar, "Exploration of adulteration in some food materials using high-sensitivity configuration of electric-LC resonator sensor," *Int. J. RF Microw. Comput.-Aided Eng.*, vol. 30, no. 2, p. 22045, Feb. 2020.

[23] V. Subramanian, V. R. K. Murthy, and J. Sobhanadri, "Sensitivity analysis of transient measurements using the microwave cavity perturbation technique," *J. Appl. Phys.*, vol. 83, no. 2, pp. 837–842, Jan. 1998.

[24] A. D. González-Monroy, T. K. Kataria, J. L. Olvera-Cervantes, A. Corona-Chávez, C. Ozuna, G. Rodríguez-Hernández, and M. E. Sosa-Morales, "Dielectric properties of beverages (tamarind and green) relevant to microwave-assisted pasteurization," *J. Food Sci.*, vol. 83, no. 9, pp. 2317–2323, Sep. 2018.

[25] D. V. B. Murthy, V. Subramanian, B. Sundaray, and T. S. Natarajan, "Microwave Hall mobility studies on polymer-single walled carbon nanotube composite fibers," *Appl. Phys. Lett.*, vol. 92, no. 22, Jun. 2008, Art. no. 222111.

[26] P. K. Varshney, A. Kapoor, and M. J. Akhtar, "Highly sensitive ELC resonator based differential sensor," *IEEE Trans. Instrum. Meas.*, vol. 70, pp. 1–10, 2021.

[27] P. K. Varshney and M. J. Akhtar, "Permittivity estimation of dielectric substrate materials via enhanced SIW sensor," *IEEE Sensors J.*, vol. 21, no. 10, pp. 12104–12112, May 2021.

[28] M. S. Boybay and O. M. Ramahi, "Material characterization using complementary split-ring resonators," *IEEE Trans. Instrum. Meas.*, vol. 61, no. 11, pp. 3039–3046, Nov. 2012.

[29] H. Lobato-Morales, D. V. B. Murthy, A. Corona-Chavez, J. L. Olvera-Cervantes, J. Martinez-Brito, and L. G. Guerrero-Ojeda, "Permittivity measurements at microwave frequencies using epsilon-near-zero (ENZ) tunnel structure," *IEEE Trans. Microw. Theory Techn.*, vol. 59, no. 7, pp. 1863–1868, Jul. 2011.

[30] S. A. Alotaibi, Y. Cui, and M. M. Tentzeris, "CSRR based sensors for relative permittivity measurement with improved and uniform sensitivity throughout [0.9–10.9] GHz band," *IEEE Sensors J.*, vol. 20, no. 9, pp. 4667–4678, May 2020.

[31] V. Sze, Y. Chen, J. Emer, A. Suleiman, and Z. Zhang, "Hardware for machine learning: Challenges and opportunities," in *Proc. IEEE Custom Integr. Circuits Conf. (CICC)*, Apr. 2018, pp. 1–8.

[32] A. Bhargava and A. Bansal, "Fruits and vegetables quality evaluation using computer vision: A review," *J. King Saud Univ. Comput. Inf. Sci.*, vol. 33, no. 3, pp. 243–257, Mar. 2021.

[33] L. Zhou, C. Zhang, F. Liu, Z. Qiu, and Y. He, "Application of deep learning in food: A review," *Comprehensive Rev. Food Sci. Food Saf.*, vol. 18, no. 6, pp. 1793–1811, Nov. 2019.

[34] L. Zhu, P. Spachos, E. Pensini, and K. N. Plataniotis, "Deep learning and machine vision for food processing: A survey," *Current Res. food Sci.*, vol. 4, pp. 233—249, Jan. 2021.

[35] Y. LeCun, K. Kavukcuoglu, and C. Farabet, "Convolutional networks and applications in vision," in *Proc. IEEE Int. Symp. Circuits Syst.*, Jun. 2010, pp. 253–256.

[36] R. Yazdani, J. Arnau, and A. González, "UNFOLD: A memory-efficient speech recognizer using on-the-fly WFST composition," in *Proc. 50th Annu. IEEE/ACM Int. Symp. Microarchitecture (MICRO)*. New York, NY, USA: Association for Computing Machinery, Oct. 2017, pp. 69–81.

[37] N. Verma, A. Shoeb, J. V. Guttag, and A. P. Chandrakasan, "A micro-power EEG acquisition SoC with integrated seizure detection processor for continuous patient monitoring," in *Proc. Symp. VLSI Circuits*, Jun. 2009, pp. 62–63.

[38] K. H. Lee and N. Verma, "A low-power processor with configurable embedded machine-learning accelerators for high-order and adaptive analysis of medical-sensor signals," *IEEE J. Solid-State Circuits*, vol. 48, no. 7, pp. 1625–1637, Jul. 2013.

[39] A. Lavin and S. Gray, "Fast algorithms for convolutional neural networks," in *Proc. IEEE Conf. Comput. Vis. Pattern Recognit.*, Jun. 2015, pp. 4013–4021.

[40] A. Gholami, S. Kim, Z. Dong, Z. Yao, M. W. Mahoney, and K. Keutzer, "A survey of quantization methods for efficient neural network inference," 2021, *arXiv:2103.13630*.

[41] D. Marculescu, D. Stamoulis, and E. Cai, "Hardware-aware machine learning: Modeling and optimization," in *Proc. IEEE/ACM Int. Conf. Comput.-Aided Design (ICCAD)*, Nov. 2018, pp. 1–8.

[42] M. Capra, B. Bussolino, A. Marchisio, G. Masera, M. Martina, and M. Shafique, "Hardware and software optimizations for accelerating deep neural networks: Survey of current trends, challenges, and the road ahead," *IEEE Access*, vol. 8, pp. 225134–225180, 2020.

[43] R. Peñaloza-Delgado, J. L. Olvera-Cervantes, M. E. Sosa-Morales, T. K. Kataria, and A. Corona-Chávez, "Dielectric characterization of vegetable oils during a heating cycle," *J. Food Sci. Technol.*, vol. 58, no. 4, pp. 1480–1487, Apr. 2021.

[44] S. O. Nelson, "Measurement and calculation of powdered mixture permittivities," *IEEE Trans. Instrum. Meas.*, vol. 50, no. 5, pp. 1066–1070, Oct. 2001.

[45] F. Pedregosa, S. Varoquaux, A. Gramfort, V. Michel, and B. Thirion, "Scikit-learn: Machine learning in Python," *J. Mach. Learn. Res.*, vol. 12, pp. 2825–2830, Dec. 2011.

[46] B. C. Schafer and Z. Wang, "High-level synthesis design space exploration: Past, present, and future," *IEEE Trans. Comput.-Aided Design Integr. Circuits Syst.*, vol. 39, no. 10, pp. 2628–2639, Oct. 2020.

[47] A. E. Eiben, P.-E. Raue, and Z. Ruttkay, "Genetic algorithms with multi-parent recombination," in *Proc. Int. Conf. Parallel Problem Solving Nature*, 1994, pp. 78–87.

[48] *MSP430 Ultra-Low-Power Sensing and Measurement MCUs, 2020*, Texas Instrum., Dallas, TX, USA, 2022.

[49] *Code Composer Studio (CCS)*, Texas Instrum., Dallas, TX, USA, 2020.
[50] *CyberWorkBench V.6.1.1*, NEC, NEX, Tokyo, Japan, 2022.
[51] *Version 9.4 (R2018A)*, MATLAB, The MathWorks Inc., Natick, MA, USA, 2018.

TEJINDER KAUR (Member, IEEE) received the B.S. degree in electronics engineering from Punjab Technical University, India, in 2003, and the M.S. degree in electronic engineering and the Ph.D. degree in electrical engineering from Instituto Nacional de Astrofisica, Optica y Electrónica, Mexico, in 2007 and 2011, respectively. From 2011 to 2013, she was a Lecturer with Universidad de las Américas Puebla, Cholula, Mexico. From 2014 to 2021, she was a Professor with Universidad de Guanajuato, Salamanca, Mexico. In 2022, she joined Universidad Autonoma de la Ciudad de Mexico, Mexico City, Mexico.

AXEL GAMEZ is currently pursuing the bachelor's degree with the Department of Electrical and Computer Engineering, The University of Texas at Dallas. His research interests include embedded systems and the use of machine learning for efficient hardware and software design.

JOSE-LUIS OLVERA-CERVANTES received the B.Sc. degree from Instituto Politécnico Nacional, Mexico City, Mexico, in 2001, and the M.Sc. and Ph.D. degrees from Centro de Investigación Científica y de Educación Superior de Ensenada, Ensenada, Mexico, in 2005 and 2008, respectively. In 2009, he joined with Instituto Nacional de Astrofísica, Óptica y Electrónica, where he is currently a Full Professor. His research interests include microwave sensors, radar systems, dielectric characterization, food properties, and signal processing.

BENJAMIN CARRION SCHAEFER (Senior Member, IEEE) received the Ph.D. degree from the University of Birmingham, U.K., in 2003.

Then, he was with the Computer Science Department, University of California at Los Angeles (UCLA), as a Postdoctoral Researcher, from 2003 to 2004, and he joined the School of Electronic Engineering and Computer Science, Seoul National University, South Korea, as a Visiting Research Scholar, from 2005 to 2007. From 2007 to September 2012, he was a Researcher with the System IP Core Department, Central Research and Development Centre, NEC Corporation, Kawasaki, Japan. From 2012 to 2016, he was an Assistant Professor with the Department of Electronic and Information Engineering (EIE), The Hong Kong Polytechnic University, where he established the Design Automation and Reconfigurable Computing Laboratory (DARClab). Since 2016, he has been an Associate Professor with the Department of Electrical and Computer Engineering, The University of Texas at Dallas. He was a recipient of the Early Career Scheme from the Research Grants Council, Hong Kong. He has been engaged in the research and development of VLSI systems, reconfigurable computing, thermal-aware VLSI design, and high-level synthesis (HLS). He has over 30 publications as the first author in international scientific journals, conferences, and books. He has served on the TPC of most EDA and FPGA conferences, including ASP-DAC, CASES, DATE, DAC, ICCAD, and FPL. He was also a member of the Accelleras SystemC synthesizable user group committee, leading the effort to standardize a synthesizable subset of SystemC.

ALONSO CORONA-CHAVEZ (Senior Member, IEEE) received the B.Sc. degree in electronics engineering from ITESM, Mexico, and the Ph.D. degree from the University of Birmingham, U.K., in 2001. His Ph.D. thesis concerned microwave beamformers using high temperature superconductors. From 2001 to 2004, he was a Microwave Engineer with CryoSystems Ltd., U.K., where he developed superconducting front ends for the telecommunications industry. Moreover, he was an Honorary Research Fellow with the Electrical Engineering Department, University of Birmingham (2001–2004). In September 2004, he joined INAOE, where he is currently a Professor with the Electronics Department. In April 2009, he was awarded a Fulbright Fellowship to carry out research with the Electrical Engineering Department, University of California at Los Angeles. He was a Visiting Professor and an Adjunct Professor with the University of Queens, Canada, in 2014, and a Professor with Universidad de Guanajuato (2015–2016). He is a member of the National Systems for Researchers (SNI).